Since January 2020 Elsevier has created a COVID-19 resource centre with free information in English and Mandarin on the novel coronavirus COVID-19. The COVID-19 resource centre is hosted on Elsevier Connect, the company's public news and information website.

Brief Report

Cell Host & Microbe

Antigenic characterization of the SARS-CoV-2 Omicron subvariant BA.2.75

Graphical abstract

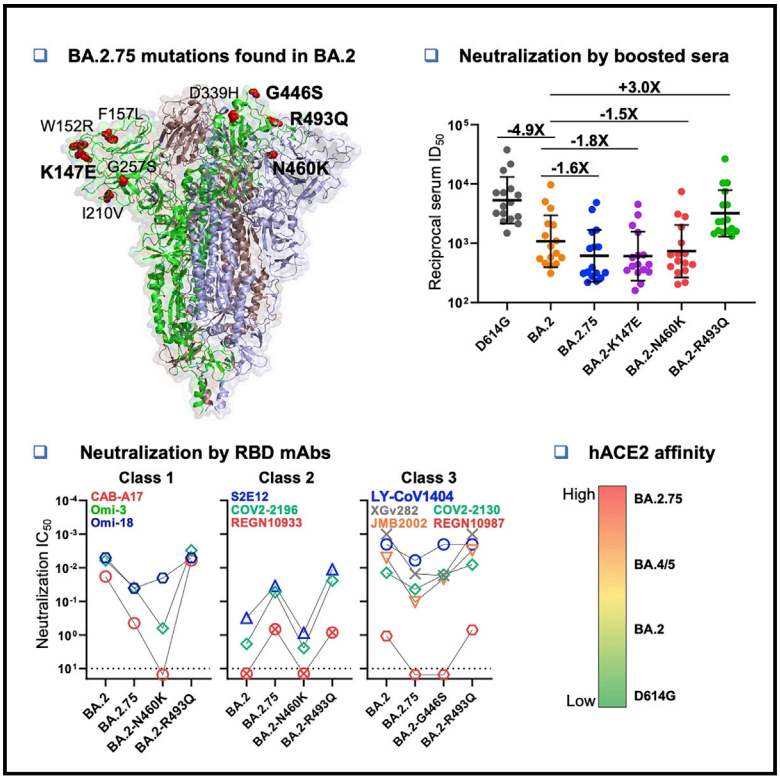

Highlights

- BA.2.75 is more resistant to neutralization by polyclonal sera than BA.2
- BA.2.75 shows heightened resistance to class 1 and class 3 RBD-directed antibodies
- BA.2.75 is the first variant to show discernible resistance to bebtelovimab
- BA.2.75 exhibits higher human ACE2-binding affinity than other Omicron subvariants

Authors

Qian Wang, Sho Iketani, Zhiteng Li, ..., Yaoxing Huang, Lihong Liu, David D. Ho

Correspondence

ll3411@cumc.columbia.edu (L.L.), dh2994@cumc.columbia.edu (D.D.H.)

In brief

Wang et al. have systematically evaluated the antigenic properties of the new SARS-CoV-2 Omicron subvariant BA.2.75. They found that BA.2.75 exhibits greater neutralization resistance to monoclonal antibodies and vaccine- and infection-induced sera than previous Omicron subvariant BA.2, while showing a higher binding affinity for human ACE2.

Wang et al., 2022, Cell Host & Microbe *30*, 1–6
November 9, 2022
https://doi.org/10.1016/j.chom.2022.09.002

CellPress

Please cite this article in press as: Wang et al., Antigenic characterization of the SARS-CoV-2 Omicron subvariant BA.2.75, Cell Host & Microbe (2022), https://doi.org/10.1016/j.chom.2022.09.002

Cell Host & Microbe

CellPress
OPEN ACCESS

Brief Report

Antigenic characterization of the SARS-CoV-2 Omicron subvariant BA.2.75

Qian Wang,[1,5] Sho Iketani,[1,5] Zhiteng Li,[1] Yicheng Guo,[1] Andre Yanchen Yeh,[2] Michael Liu,[1] Jian Yu,[1] Zizhang Sheng,[1] Yaoxing Huang,[1] Lihong Liu,[1,*] and David D. Ho[1,3,4,6,*]

[1]Aaron Diamond AIDS Research Center, Columbia University Vagelos College of Physicians and Surgeons, New York, NY 10032, USA
[2]School of Medicine, National Taiwan University, Taipei 100233, Taiwan
[3]Department of Microbiology and Immunology, Columbia University Vagelos College of Physicians and Surgeons, New York, NY 10032, USA
[4]Division of Infectious Diseases, Department of Medicine, Columbia University Vagelos College of Physicians and Surgeons, New York, NY 10032, USA
[5]These authors contributed equally
[6]Lead contact
*Correspondence: ll3411@cumc.columbia.edu (L.L.), dh2994@cumc.columbia.edu (D.D.H.)
https://doi.org/10.1016/j.chom.2022.09.002

SUMMARY

The severe acute respiratory syndrome coronavirus 2 (SARS-CoV-2) Omicron subvariant BA.2.75 emerged recently and appears to be spreading. It has nine mutations in spike compared with the currently circulating BA.2, raising concerns that it may further evade vaccine-elicited and therapeutic antibodies. We found BA.2.75 to be moderately more neutralization resistant to sera from vaccinated/boosted individuals than BA.2 (1.8-fold), similar to BA.2.12.1 (1.1-fold), but more neutralization sensitive than BA.4/5 (0.6-fold). Relative to BA.2, BA.2.75 showed heightened resistance to class 1 and class 3 monoclonal antibodies targeting the spike-receptor-binding domain while gaining sensitivity to class 2 antibodies. Resistance was largely conferred by G446S and R460K mutations. BA.2.75 was slightly resistant (3.7-fold) to bebtelovimab, a therapeutic antibody with potent activity against all Omicron subvariants. BA.2.75 also exhibited a higher binding affinity to host receptor ACE2 than other Omicron subvariants. BA.2.75 provides further insight into SARS-CoV-2 evolution as it gains transmissibility while incrementally evading antibody neutralization.

The coronavirus disease 2019 (COVID-19) pandemic is currently dominated by the severe acute respiratory syndrome coronavirus 2 (SARS-CoV-2) Omicron subvariant BA.5. Yet, another subvariant known as BA.2.75 has recently emerged from India, where it has spread rapidly, displacing the predominant BA.2 subvariant locally. Moreover, BA.2.75 has now been identified in at least 27 countries worldwide (Shu and McCauley, 2017) (Figure S1A). Though a descendent from BA.2, it contains a distinct set of mutations in its spike protein, including five substitutions in the N-terminal domain (NTD), K147E, W152R, F157L, I210V, and G257S, and four substitutions in the receptor-binding domain (RBD), D339H, G446S, N460K, and R493Q (Figure S1B). Many of these mutations are located at sites targeted by neutralizing antibodies and may also affect the binding affinity of the spike to its receptor, angiotensin-converting enzyme 2 (ACE2). In particular, two RBD mutations, D339H and N460K, are noteworthy because they have not been identified in previous SARS-CoV-2 variants and their impacts are not yet known. Newfound variants such as BA.2.75 that are increasing in frequency raise the concern that the viruses have developed additional mechanisms to escape from neutralization by antibodies elicited by vaccination or previous infection, as well as by therapeutic monoclonal antibodies (mAbs) in clinical use. Therefore, we have evaluated the antibody evasion properties of BA.2.75, and our findings are reported here.

We first set out to profile the antigenic differences of BA.2.75 from the wild-type SARS-CoV-2 D614G and the other currently circulating Omicron subvariants BA.2, BA.2.12.1, and BA.4/5 (note that BA.4 and BA.5 share an identical spike). Vesicular stomatitis virus (VSV)—pseudotyped viruses of each variant—were produced and then assessed for their neutralization sensitivity to sera from three different clinical cohorts: those who had received three doses of a COVID-19 mRNA vaccine (boosted) and patients with either BA.1 or BA.2 breakthrough infection after vaccination. We did not include sera from persons immunized with only two doses of COVID-19 mRNA vaccines as we had previously observed that they lacked neutralization capacity against earlier Omicron subvariants (Iketani et al., 2022; Liu et al., 2022b). The clinical information for our cohorts is described in Table S1, and the serum neutralization profiles are shown in Figure 1A. Consistent with previous reports (Iketani et al., 2022; Liu et al., 2022b; Wang et al., 2022b), neutralization ID_{50} (the 50% inhibitory dose) titers of the "boosted" sera were substantially lower against BA.2, BA.2.12.1, and BA.4/5 (4.9-, 7.8-, and 14.8-fold, respectively), compared with D614G. Neutralization titers against BA.2.75 were similar to those against BA.2.12.1,

Please cite this article in press as: Wang et al., Antigenic characterization of the SARS-CoV-2 Omicron subvariant BA.2.75, Cell Host & Microbe (2022), https://doi.org/10.1016/j.chom.2022.09.002

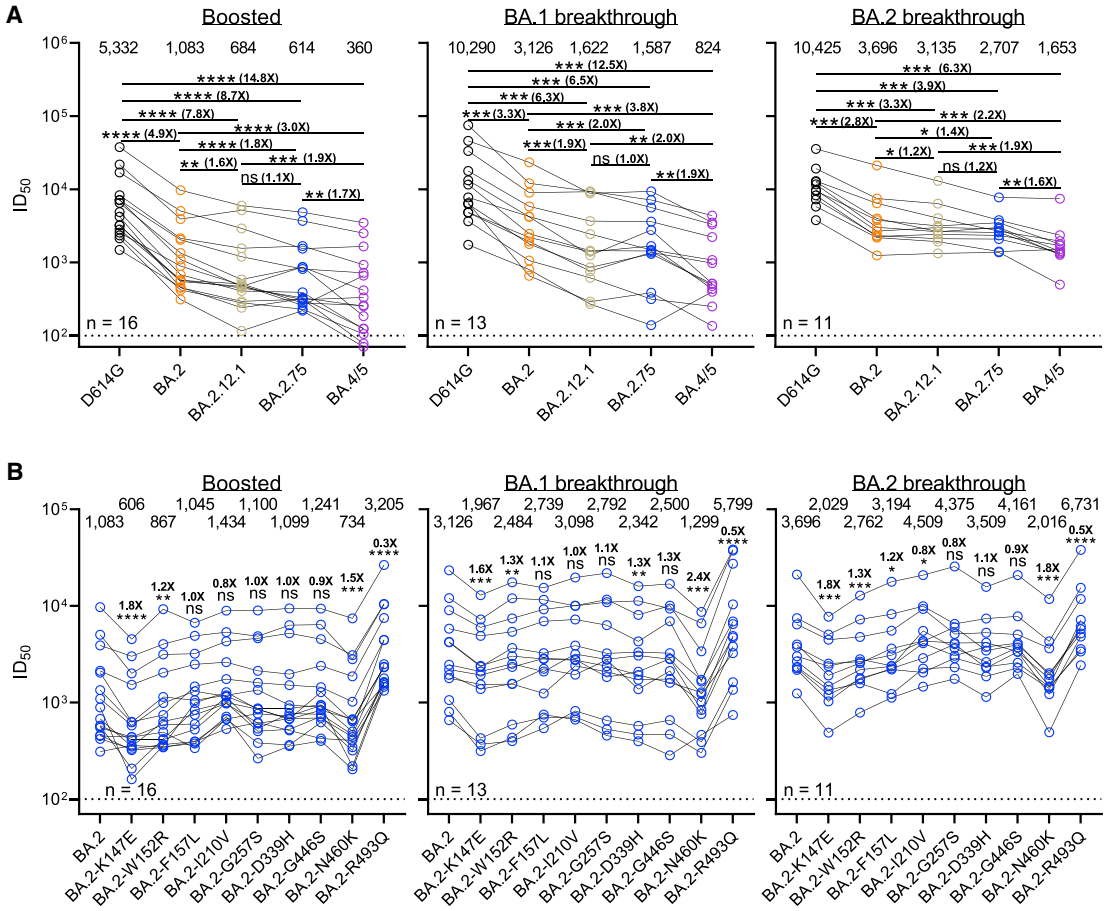

Figure 1. Serum neutralization profile of BA.2.75

(A) Neutralization of pseudotyped D614G and Omicron subvariants by sera from three different clinical cohorts. Boosted refers to individuals who received three doses of a COVID-19 mRNA vaccine, and breakthrough refers to individuals who were infected and received COVID-19 vaccines.

(B) Serum neutralization of pseudotyped BA.2 or BA.2 with point mutations from BA.2.75. For both panels, values above the symbols denote the geometric mean ID_{50} values and values on the lower left indicate the sample size (n) for each group. The limit of detection (LOD) is 100 (dotted line), and values below the LOD are arbitrarily plotted to allow for visualization of each sample. The p values were determined by using two-tailed Wilcoxon matched-pairs signed-rank tests. In (B), comparisons were made against BA.2. Significance is denoted with asterisks, and the fold change is also denoted. Ns, not significant; *$p < 0.05$; **$p < 0.01$; ***$p < 0.001$; and ****$p < 0.0001$.

See also Figure S1 and Table S1.

8.7-fold lower than D614G, 1.8-fold lower than BA.2, but 1.7-fold higher than BA.4/5. A similar trend was observed in the "BA.1 and BA.2 breakthrough" cohorts.

We also investigated the impact of new point mutations found in BA.2.75 on serum antibody evasion by conducting serum neutralization assays with pseudoviruses containing each point mutation in the background of BA.2 (Figure 1B). The mutations W152R, F157L, I210V, G257S, D339H, and N446K each only slightly (0.8- to 1.3-fold) altered the neutralization titers of sera from all three cohorts against BA.2. By contrast, K147E and N460K impaired the neutralization activity of sera significantly, by 1.6- to 1.8-fold and 1.5- to 2.4-fold, respectively, whereas the R493Q reversion mutation modestly enhanced the neutralization by 1.8- to 3.0-fold, as was observed previously (Wang et al., 2022b).

We next assessed the neutralization resistance of BA.2.75 to a panel of 23 mAbs directed to known neutralizing epitopes on the viral spike. Among these, 21 target the four epitope classes in the RBD (Barnes et al., 2020), including REGN10987 (imdevimab) (Hansen et al., 2020), REGN10933 (casirivimab) (Hansen et al., 2020), COV2-2196 (tixagevimab) (Zost et al., 2020), COV2-2130 (cilgavimab) (Zost et al., 2020), LY-CoV555 (bamlanivimab) (Jones et al., 2021), CB6 (etesevimab) (Shi et al., 2020), Brii-196 (amubarvimab) (Ju et al., 2020), Brii-198 (romlusevimab) (Ju et al., 2020), S309 (sotrovimab) (Pinto et al., 2020), LY-CoV1404 (bebtelovimab) (Westendorf et al., 2022), CAB-A17 (Sheward et al., 2022), ZCB11 (Zhou et al., 2022), Omi-3 (Nutalai et al., 2022), Omi-18 (Nutalai et al., 2022), XGv282 (Wang et al., 2022a), XGv347 (Wang et al., 2022a), S2E12 (Starr et al., 2021), A19-46.1 (Wang et al., 2021), 35B5 (Wang et al., 2022c), and JMB2002 (Yin et al., 2022), as well as 10-40 (Liu et al., 2022a) from our group. The other two mAbs, C1717 (Wang et al., 2022d) and S3H3 (Hong et al., 2022), target NTD-SD2 and SD1, respectively. Many of the recently isolated mAbs were chosen because they could neutralize earlier Omicron subvariants

Please cite this article in press as: Wang et al., Antigenic characterization of the SARS-CoV-2 Omicron subvariant BA.2.75, Cell Host & Microbe (2022), https://doi.org/10.1016/j.chom.2022.09.002

CellPress
OPEN ACCESS

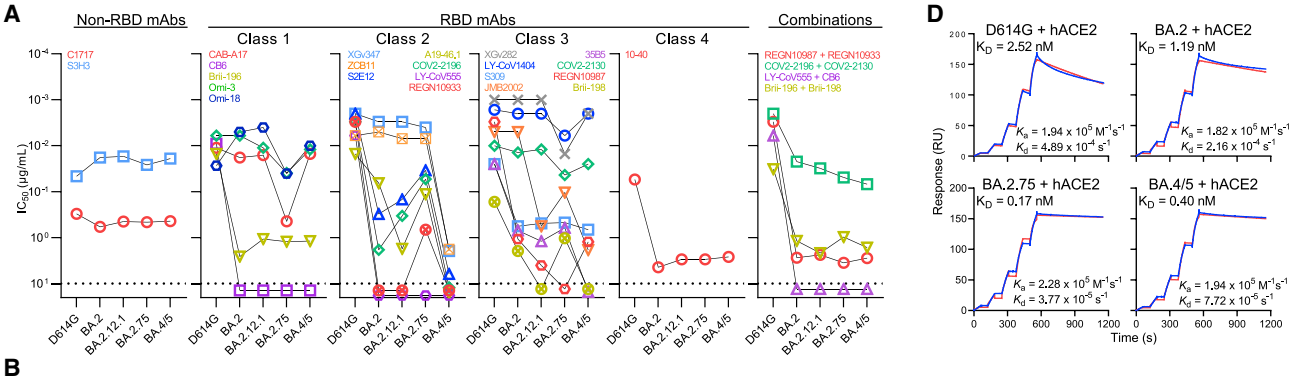

B

	Fold change in IC_{50}	NTD-SD2	SD1	RBD mAbs																					Combinations			
				Class 1					Class 2							Class 3								Class 4				
		C1717	S3H3	CAB-A17	CB6	Brii-196	Omi-3	Omi-18	XGv347	ZCB11	S2E12	A19-46.1	COV2-2196	LY-CoV 555	REGN 10933	XGv282	LY-CoV 1404	S309	35B5	JMB 2002	COV2-2130	REGN 10987	Brii-198	10-40	REGN10987 + REGN10933	COV2-2196 + COV2-2130	LY-CoV555 + CB6	Brii-196 + Brii-198
Compared with D614G	D614G-K147E	-1.0	1.2	1.3	1.0	1.1	1.1	1.1	-1.0	1.4	1.5	1.2	1.4	1.7	1.2	1.1	1.2	-1.1	1.0	-1.3	1.5	1.4	-1.7	-1.4	-1.1	-1.5	1.1	-1.0
	D614G-W152R	1.0	1.1	1.2	-1.0	-1.5	-1.4	-1.3	1.2	-1.0	1.3	1.1	1.1	1.3	-1.0	-1.3	-1.3	-1.2	1.4	-1.5	1.1	1.1	1.0	-1.0	-1.2	-1.4	-1.1	-1.0
	D614G-F157L	1.1	1.5	1.3	1.3	1.2	1.5	2.4	1.5	2.0	2.2	2.8	1.2	2.0	1.7	1.0	1.3	-1.2	1.3	-1.1	1.8	-1.1	-1.4	-1.2	1.1	-1.2	1.5	1.5
	D614G-I210V	1.1	1.3	1.1	1.1	1.1	-1.2	1.5	1.0	1.1	1.6	1.5	1.0	1.5	1.1	-1.1	1.1	1.1	1.4	-1.3	1.3	-1.0	-1.8	-1.2	1.1	-1.5	-1.2	1.2
	D614G-G257S	-1.2	1.8	1.2	1.1	1.3	-1.2	1.2	1.4	1.2	1.1	1.6	1.6	1.4	1.1	-1.1	-1.1	-1.1	1.3	-1.4	-1.0	-1.3	-1.2	-1.4	-1.1	-1.3	-1.1	1.3
	D614G-G339H	1.1	1.6	1.1	1.1	-1.3	-1.6	1.2	-1.2	-1.2	-1.0	1.4	1.0	1.3	1.0	-1.4	1.1	-1.1	1.1	-1.5	1.3	-1.4	-1.3	-1.5	-1.6	-1.5	-1.3	-1.0
	D614G-G446S	1.1	2.0	1.2	1.2	1.1	1.1	1.3	1.0	1.1	1.3	-1.5	1.1	1.2	1.2	-3.5	-1.9	1.3	-1.0	-27	-3.1	-2462	-1.1	1.2	-4.0	-2.5	-1.1	1.4
	D614G-N460K	1.0	1.9	-1.2	-172	-8.6	-1.9	-1.2	-1.1	-1.0	-1.0	-1.5	-1.1	1.3	-1.4	-1.3	1.0	-1.1	-1.1	-1.6	1.2	-1.2	-2.4	-1.7	-1.3	-1.7	-1.7	-4.7
Compared with BA.2	BA.2-K147E	1.1	-1.3	-2.4	NA	1.3	-2.2	-1.1	-1.4	-2.7	-1.4	1.1	-1.2	NA	NA	-1.6	1.0	1.0	1.2	1.2	1.2	-1.5	1.0	-1.0	1.4	-1.2	NA	-1.3
	BA.2-W152R	1.5	1.4	-1.4	NA	1.8	-1.7	1.2	1.3	-1.7	1.5	2.0	1.1	NA	NA	-1.1	1.4	1.5	3.2	1.1	1.1	1.4	1.4	1.6	1.5	1.1	NA	-1.2
	BA.2-F157L	-1.0	1.1	-1.8	NA	1.9	-2.0	-1.3	-1.1	-2.4	-1.2	1.0	-1.7	NA	NA	1.0	1.6	-1.0	-1.0	1.4	1.2	1.8	1.4	3.8	1.0	-1.2	NA	-1.5
	BA.2-I210V	1.6	-1.0	-1.6	NA	1.5	-1.9	-1.2	-1.1	-1.6	1.0	1.3	2.1	NA	NA	-1.3	1.1	1.1	1.1	1.3	1.1	-1.3	1.5	1.5	1.5	1.3	NA	1.3
	BA.2-G257S	1.2	1.2	-1.8	NA	-2.1	-2.4	-1.3	1.1	-2.1	1.0	1.3	1.3	NA	NA	1.6	1.2	1.5	1.2	1.3	1.3	1.0	1.3	2.0	2.6	1.6	NA	-1.0
	BA.2-D339H	1.1	-1.0	-1.6	NA	1.5	-1.6	1.2	1.4	-2.3	1.1	1.3	-1.2	NA	NA	-1.0	1.3	2.4	1.5	1.5	1.2	1.0	1.9	2.1	1.1	1.1	NA	-1.0
	BA.2-G446S	-1.0	1.7	1.0	NA	1.8	-1.3	-1.1	1.0	-2.2	-1.0	-1.0	1.6	NA	NA	-14	1.1	1.2	1.4	-4.1	-1.2	<-9.4	1.1	1.0	<-3.7	-1.2	NA	1.5
	BA.2-N460K	-2.1	1.2	<-558	NA	<-3.9	-75	-4.3	-1.2	-35	-2.8	-1.5	-1.3	NA	NA	1.1	1.2	-1.3	-2.5	-1.3	-1.2	-2.8	-1.8	<-2.3	-1.8	1.0	NA	<-8.6
	BA.2-R493Q	2.2	-1.2	3.2	NA	150	2.4	-1.1	2.9	3.6	29	3.0	76	NA	>12	2.4	1.2	1.3	2.9	1.7	1.7	1.5	1.5	3.0	3.8	1.8	NA	23.4

>10 >3 <-3 <-10 <-100 <-1000

C

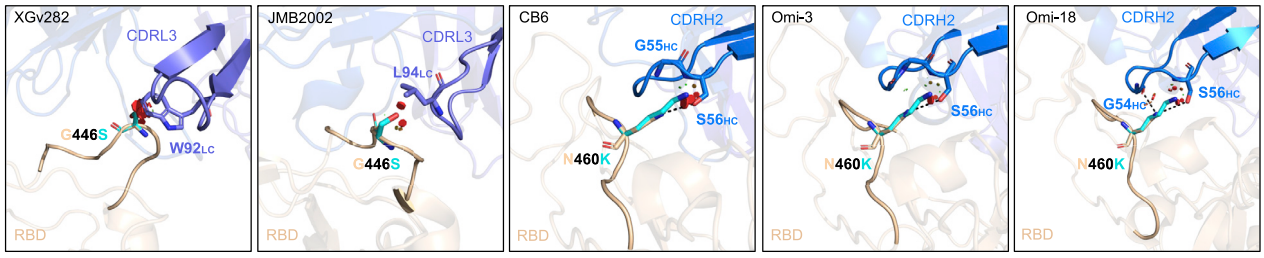

Figure 2. Neutralization of BA.2.75 by monoclonal antibodies and receptor-binding affinity

(A) Neutralization of pseudotyped D614G and Omicron subvariants by NTD-SD2-, SD1-, and RBD-directed mAbs. Values above the LOD of 10 μg/mL (dotted line) are arbitrarily plotted to allow for visualization of each sample.

(B) Fold change in IC_{50} values for the neutralization of pseudotyped point mutants, relative to D614G or BA.2, with resistance colored red and sensitization colored green. NA, not applicable.

(C) Modeling of the impact of G446S and N460K on antibody neutralization. Clashes are shown as red discs, and hydrogen bonds are shown as dashed lines.

(D) Binding affinity of D614G, BA.2, BA.2.75, and BA.4/5 stabilized spike trimers to dimeric human ACE2.

See also Figures S1 and S2 and Table S2.

(Hong et al., 2022; Nutalai et al., 2022; Sheward et al., 2022; Starr et al., 2021; Wang et al., 2021, 2022a, 2022c, 2022d; Yin et al., 2022; Zhou et al., 2022).

The results are presented in Figure 2A and Table S2. Unlike BA.2.12.1, which was largely similar in its antigenic profile to BA.2, BA.2.75 differed from BA.2 across a wide range of the mAbs tested. Antibodies across multiple classes were impaired against BA.2.75 compared with BA.2, including some in class 1 (CAB-A17, Omi-3, and Omi-18) and class 3 (XGv282, LY-CoV1404, JMB2002, COV2-2130, and REGN10987). Simultaneously, several antibodies showed neutralization sensitivity against BA.2.75 relative to BA.2, all within class 2 (S2E12, COV2-2196, and REGN10933). This also contrasts that of BA.4/5, which demonstrated heightened resistance to class 2 and class 3 antibodies over BA.2. Moreover, even within the resistance to class 3 antibodies, BA.2.75 and BA.4/5 only overlapped with additional resistance toward one antibody, JMB2002. The other impaired antibodies differed, with 35B5 and Brii-198 losing further activity against BA.4/5 over BA.2. These data suggest that BA.2.75 has evolved to extend resistance toward some class 1- and class 3-directed antibodies over BA.2 yet has regained sensitivity for a subset of class 2 antibodies. Such differences may help to interpret the observations made on polyclonal serum neutralization (Figure 1).

Of particular note, BA.2.75 is the first SARS-CoV-2 variant that has demonstrated resistance to bebtelovimab (LY-CoV1404),

Please cite this article in press as: Wang et al., Antigenic characterization of the SARS-CoV-2 Omicron subvariant BA.2.75, Cell Host & Microbe (2022), https://doi.org/10.1016/j.chom.2022.09.002

albeit modestly at a 3.7-fold loss in neutralization (Figure 2A). Nevertheless, it remained the only clinical mAb that retained potent neutralizing activity against all the Omicron subvariants with an IC_{50} (the 50% inhibitory concentration) below 0.01 μg/mL. All other clinically authorized or approved antibodies or antibody combinations showed a substantial loss of activity *in vitro* against BA.2.75.

As we observed that BA.2.75 was resistant to mAbs in a unique way, we set out to identify the mutations within BA.2.75 that conferred the observed antibody resistance profile. We generated pseudoviruses carrying each of the point mutations in the background of D614G or BA.2 and tested their neutralization sensitivity to the aforementioned panel of mAbs and combinations. These data are shown in Figure 2B and Table S2. G446S impaired or abolished the neutralizing activity of class 3 mAbs (XGv282, JMB2002, and REGN10987), as previously observed in our BA.1 studies (Liu et al., 2022b). That this mutation did not result in a significant loss in polyclonal serum neutralization (Figure 1B) suggests that such antibodies may be rare in a polyclonal response. The N460K substitution conferred resistance to all of the class 1 RBD mAbs tested, as well as one class 2 mAb (ZCB11). However, this resistance was only observed in the context of BA.2 for three of the class 1 antibodies (CAB-A17, Omi-3, and Omi-18) and the class 2 antibody ZCB11 but not in the context of D614G. By contrast, R493Q, also found in BA.4/5 (Wang et al., 2022b), sensitized BA.2 to neutralization by several class 1 and 2 RBD mAbs, which is consistent with our previous study (Wang et al., 2022b). We note that although the NTD mutation K147E had a significant impact on polyclonal sera (Figure 1B), we did not observe an effect by this mutation against the panel of mAbs tested here, suggesting that this mutation may be acting through non-RBD antibodies.

We conducted structural modeling to further investigate the impact of the G446S and N460K mutations (Figure 2C). Analysis of G446S revealed steric hindrance to binding by class 3 RBD mAbs (XGv282 and JMB2002), as we reported previously (Liu et al., 2022b). In addition, structural modeling of N460K revealed that K460 abolished a common hydrogen bond between RBD-N460 and S56 in CDRH2 of VH3-53 class antibodies (Barnes et al., 2020), such as CB6, Omi-3, and Omi-18, although it is not immediately clear why the loss in activity for Omi-3 and Omi-18 was only apparent in the background of BA.2 but not D614G.

Finally, as receptor-binding affinity may play a role in transmissibility, we investigated this property for BA.2.75. The binding affinity of purified spike trimer proteins of D614G, BA.2, BA.4/5, and BA.2.75 to dimeric human ACE2 (hACE2) was quantified using surface plasmon resonance (SPR). We found that BA.2.75 exhibited the highest receptor-binding affinity, with a K_D value 7.0- and 2.4-fold lower than values for BA.2 and BA.4/5, respectively (Figure 2D). To validate these results, we tested pseudoviruses bearing these spikes for neutralization by dimeric hACE2 (Figure S2). A comparison of IC_{50} values suggested that BA.2.75 was slightly more sensitive to hACE2 than the other pseudoviruses tested, in line with what was observed in the SPR. To probe the role of the mutations in BA.2.75 for ACE2 binding, we tested the neutralization by hACE2 of each of the point mutants in the background of BA.2. R493Q was the most sensitive to hACE2 neutralization, and N460K was the most resistant. These results parallel our previous studies in which we found R493Q could serve to restore the lost receptor-binding affinity due to a resistance-conferring mutation in BA.4/5 (Wang et al., 2022b). A similar mechanism in which R493Q acts to balance the compromised affinity caused by N460K may be in action for BA.2.75.

In summary, we have systematically evaluated the antigenic properties of the new SARS-CoV-2 Omicron subvariant BA.2.75, which is spreading throughout the world. Our data suggest that BA.2.75 exhibits higher resistance to vaccine-induced and infection-induced serum neutralizing activity than BA.2 (Figure 1A). It is reassuring that BA.2.75 does not show greater immune evasion from polyclonal sera than the BA.4/5 subvariant (Figure 1A). The resistance profile of BA.2.75 to sera can be largely attributed to the K147E and N460K mutations (Figure 1B). The latter mutation is consistent with findings from deep mutational scanning of the RBD (Greaney et al., 2021b). The impact of the former mutation is puzzling in that previous Omicron subvariants have already abolished the activity of the antibodies directed to the NTD antigenic supersite (Iketani et al., 2022; Liu et al., 2022b; Wang et al., 2022b), and yet, this new variant evolved to contain five additional NTD mutations. Why is SARS-CoV-2 doing so when NTD antibodies contribute only a small portion of the serum virus-neutralizing activity (Garrett et al., 2021; Greaney et al., 2021a)?

BA.2.75 exhibits a unique neutralizing profile for mAbs, with heightened resistance over BA.2 to class 1 and class 3 RBD antibodies while gaining sensitivity toward class 2 RBD antibodies (Figure 2A). Although the impairment is slight, BA.2.75 is the first SARS-CoV-2 variant to show discernible resistance to bebtelovimab (LY-CoV1404). The profiling of the individual mutations within BA.2.75 revealed that G446S and N460K could contribute to the resistance (Figure 2B). These mutations appear to be acting through steric hindrance or abrogation of a hydrogen bond (Figure 2C). More importantly, these findings on BA.2.75 demonstrate that our one remaining therapeutic antibody with potent activity to treat COVID-19 is now under threat. Another mutation proximal to residue 446 of the spike could knock out the current arsenal of therapeutic monoclonals. Although numerous mAbs have been isolated and shown to neutralize the new Omicron subvariants (Hong et al., 2022; Nutalai et al., 2022; Sheward et al., 2022; Starr et al., 2021; Wang et al., 2021, 2022a, 2022c, 2022d; Yin et al., 2022; Zhou et al., 2022), their development pathway to prove clinical efficacy has become rather daunting with the availability of effective vaccines and antiviral drugs.

Finally, our data demonstrate that BA.2.75 has enhanced binding affinity to its receptor ACE2, which may enhance its transmission (Figure 2D). However, it is still unclear whether BA.2.75 could outcompete BA.5, today's dominant form globally. The features of BA.2.75 that diverged from other Omicron subvariants serve to underscore the ability of SARS-CoV-2 to evolve, incrementally gaining transmissibility and antibody evasion, and to reinforce the importance of vaccination and booster campaigns as well as epidemiologic surveillance to detect the emergence of new SARS-CoV-2 variants.

STAR★METHODS

Detailed methods are provided in the online version of this paper and include the following:

- KEY RESOURCES TABLE

SUPPLEMENTAL INFORMATION

Supplemental information can be found online at https://doi.org/10.1016/j.chom.2022.09.002.

ACKNOWLEDGMENTS

This study was supported by funding from the Gates Foundation, JPB Foundation, Andrew and Peggy Cherng, Samuel Yin, Carol Ludwig, David and Roger Wu, Regeneron Pharmaceuticals, and the NIH SARS-CoV-2 Assessment of Viral Evolution (SAVE) Program. We are grateful to Michael T. Yin, Magdalena E. Sobieszczyk, Jennifer Y. Chang, Jayesh G. Shah, and David S. Perlin for providing serum samples from COVID-19 patients. We thank all who have contributed their data to GISAID.

AUTHOR CONTRIBUTIONS

D.D.H. and L.L. conceived this project. Q.W., A.Y.Y., and L.L. constructed the spike expression plasmids and produced pseudoviruses. Q.W., S.I., and L.L. conducted the pseudovirus neutralization experiments. Q.W., Z.L., A.Y.Y., and L.L. purified the SARS-CoV-2 spike and ACE2 proteins and performed SPR. Y.G. and Z.S. conducted bioinformatic analyses. Q.W. managed the project. J.Y. and M.L. produced antibodies. D.D.H. and L.L. directed and supervised the project. Q.W., S.I., Y.G., L.L., and D.D.H. analyzed the results and wrote the manuscript.

DECLARATION OF INTERESTS

S.I., J.Y., Y.H., L.L., and D.D.H. are inventors on patent applications (WO2021236998) or provisional patent applications (63/271,627) filed by Columbia University for a number of SARS-CoV-2 neutralizing antibodies described in this manuscript. Both sets of applications are under review. D.D.H. is a co-founder of TaiMed Biologics and RenBio, consultant to WuXi Biologics and Brii Biosciences, and board director for Vicarious Surgical.

Received: August 4, 2022
Revised: August 29, 2022
Accepted: September 1, 2022
Published: September 6, 2022

REFERENCES

Barnes, C.O., Jette, C.A., Abernathy, M.E., Dam, K.A., Esswein, S.R., Gristick, H.B., Malyutin, A.G., Sharaf, N.G., Huey-Tubman, K.E., Lee, Y.E., et al. (2020). SARS-CoV-2 neutralizing antibody structures inform therapeutic strategies. Nature *588*, 682–687.

Chan, K.K., Dorosky, D., Sharma, P., Abbasi, S.A., Dye, J.M., Kranz, D.M., Herbert, A.S., and Procko, E. (2020). Engineering human ACE2 to optimize binding to the spike protein of SARS coronavirus 2. Science *369*, 1261–1265.

Garrett, M.E., Galloway, J., Chu, H.Y., Itell, H.L., Stoddard, C.I., Wolf, C.R., Logue, J.K., McDonald, D., Weight, H., Matsen, F.A., 4th, and Overbaugh, J. (2021). High-resolution profiling of pathways of escape for SARS-CoV-2 spike-binding antibodies. Cell *184*, 2927–2938.e11.

Greaney, A.J., Loes, A.N., Crawford, K.H.D., Starr, T.N., Malone, K.D., Chu, H.Y., and Bloom, J.D. (2021a). Comprehensive mapping of mutations in the SARS-CoV-2 receptor-binding domain that affect recognition by polyclonal human plasma antibodies. Cell Host Microbe *29*, 463–476.e6.

Greaney, A.J., Starr, T.N., Barnes, C.O., Weisblum, Y., Schmidt, F., Caskey, M., Gaebler, C., Cho, A., Agudelo, M., Finkin, S., et al. (2021b). Mapping mutations to the SARS-CoV-2 RBD that escape binding by different classes of antibodies. Nat. Commun. *12*, 4196.

Hansen, J., Baum, A., Pascal, K.E., Russo, V., Giordano, S., Wloga, E., Fulton, B.O., Yan, Y., Koon, K., Patel, K., et al. (2020). Studies in humanized mice and convalescent humans yield a SARS-CoV-2 antibody cocktail. Science *369*, 1010–1014.

Hong, Q., Han, W., Li, J., Xu, S., Wang, Y., Xu, C., Li, Z., Wang, Y., Zhang, C., Huang, Z., and Cong, Y. (2022). Molecular basis of receptor binding and antibody neutralization of Omicron. Nature *604*, 546–552.

Iketani, S., Liu, L., Guo, Y., Liu, L., Chan, J.F., Huang, Y., Wang, M., Luo, Y., Yu, J., Chu, H., et al. (2022). Antibody evasion properties of SARS-CoV-2 Omicron sublineages. Nature *604*, 553–556.

Jones, B.E., Brown-Augsburger, P.L., Corbett, K.S., Westendorf, K., Davies, J., Cujec, T.P., Wiethoff, C.M., Blackbourne, J.L., Heinz, B.A., Foster, D., et al. (2021). The neutralizing antibody, LY-CoV555, protects against SARS-CoV-2 infection in nonhuman primates. Sci. Transl. Med. *13*, eabf1906.

Ju, B., Zhang, Q., Ge, J., Wang, R., Sun, J., Ge, X., Yu, J., Shan, S., Zhou, B., Song, S., et al. (2020). Human neutralizing antibodies elicited by SARS-CoV-2 infection. Nature *584*, 115–119.

Liu, L., Iketani, S., Guo, Y., Casner, R.G., Reddem, E.R., Nair, M.S., Yu, J., Chan, J.F., Wang, M., Cerutti, G., et al. (2022a). An antibody class with a common CDRH3 motif broadly neutralizes sarbecoviruses. Sci Transl Med *584*, eabn6859.

Liu, L., Iketani, S., Guo, Y., Chan, J.F., Wang, M., Liu, L., Luo, Y., Chu, H., Huang, Y., Nair, M.S., et al. (2022b). Striking antibody evasion manifested by the Omicron variant of SARS-CoV-2. Nature *602*, 676–681.

Liu, L., Wang, P., Nair, M.S., Yu, J., Rapp, M., Wang, Q., Luo, Y., Chan, J.F., Sahi, V., Figueroa, A., et al. (2020). Potent neutralizing antibodies against multiple epitopes on SARS-CoV-2 spike. Nature *584*, 450–456.

Nutalai, R., Zhou, D., Tuekprakhon, A., Ginn, H.M., Supasa, P., Liu, C., Huo, J., Mentzer, A.J., Duyvesteyn, H.M.E., Dijokaite-Guraliuc, A., et al. (2022). Potent cross-reactive antibodies following Omicron breakthrough in vaccinees. Cell *185*, 2116–2131.e18.

Pinto, D., Park, Y.J., Beltramello, M., Walls, A.C., Tortorici, M.A., Bianchi, S., Jaconi, S., Culap, K., Zatta, F., De Marco, A., et al. (2020). Cross-neutralization of SARS-CoV-2 by a human monoclonal SARS-CoV antibody. Nature *583*, 290–295.

Sheward, D.J., Pushparaj, P., Das, H., Kim, C., Kim, S., Hanke, L., Dyrdak, R., McInerney, G., Albert, J., Murrell, B., et al. (2022). Structural basis of Omicron neutralization by affinity-matured public antibodies. Preprint at bioRxiv. https://doi.org/10.1101/2022.01.03.474825.

Shi, R., Shan, C., Duan, X., Chen, Z., Liu, P., Song, J., Song, T., Bi, X., Han, C., Wu, L., et al. (2020). A human neutralizing antibody targets the receptor-binding site of SARS-CoV-2. Nature *584*, 120–124.

Shu, Y., and McCauley, J. (2017). GISAID: global initiative on sharing all influenza data - from vision to reality. Euro Surveill. *22*, 30494.

Starr, T.N., Czudnochowski, N., Liu, Z., Zatta, F., Park, Y.J., Addetia, A., Pinto, D., Beltramello, M., Hernandez, P., Greaney, A.J., et al. (2021). SARS-CoV-2 RBD antibodies that maximize breadth and resistance to escape. Nature *597*, 97–102.

Wang, K., Jia, Z., Bao, L., Wang, L., Cao, L., Chi, H., Hu, Y., Li, Q., Zhou, Y., Jiang, Y., et al. (2022a). Memory B cell repertoire from triple vaccinees against diverse SARS-CoV-2 variants. Nature *603*, 919–925.

Wang, L., Zhou, T., Zhang, Y., Yang, E.S., Schramm, C.A., Shi, W., Pegu, A., Oloniniyi, O.K., Henry, A.R., Darko, S., et al. (2021). Ultrapotent antibodies against diverse and highly transmissible SARS-CoV-2 variants. Science *373*, eabh1766.

Wang, Q., Guo, Y., Iketani, S., Nair, M.S., Li, Z., Mohri, H., Wang, M., Yu, J., Bowen, A.D., Chang, J.Y., et al. (2022b). Antibody evasion by SARS-CoV-2 Omicron subvariants BA.2.12.1, BA.4 and BA.5. Nature *608*, 603–608.

Wang, X., Chen, X., Tan, J., Yue, S., Zhou, R., Xu, Y., Lin, Y., Yang, Y., Zhou, Y., Deng, K., et al. (2022c). 35B5 antibody potently neutralizes SARS-CoV-2 Omicron by disrupting the N-glycan switch via a conserved spike epitope. Cell Host Microbe *30*, 887–895.e4.

Wang, Z., Muecksch, F., Cho, A., Gaebler, C., Hoffmann, H.H., Ramos, V., Zong, S., Cipolla, M., Johnson, B., Schmidt, F., et al. (2022d). Analysis of memory B cells identifies conserved neutralizing epitopes on the N-terminal domain of variant SARS-Cov-2 spike proteins. Immunity *55*, 998–1012.e8.

Westendorf, K., Žentelis, S., Wang, L., Foster, D., Vaillancourt, P., Wiggin, M., Lovett, E., van der Lee, R., Hendle, J., Pustilnik, A., et al. (2022). LY-CoV1404 (bebtelovimab) potently neutralizes SARS-CoV-2 variants. Cell Rep. *39*, 110812.

Wrapp, D., Wang, N., Corbett, K.S., Goldsmith, J.A., Hsieh, C.L., Abiona, O., Graham, B.S., and McLellan, J.S. (2020). Cryo-EM structure of the 2019-nCoV spike in the prefusion conformation. Science *367*, 1260–1263.

Yin, W., Xu, Y., Xu, P., Cao, X., Wu, C., Gu, C., He, X., Wang, X., Huang, S., Yuan, Q., et al. (2022). Structures of the Omicron spike trimer with ACE2 and an anti-Omicron antibody. Science *375*, 1048–1053.

Zhou, B., Zhou, R., Tang, B., Chan, J.F., Luo, M., Peng, Q., Yuan, S., Liu, H., Mok, B.W., Chen, B., et al. (2022). A broadly neutralizing antibody protects Syrian hamsters against SARS-CoV-2 Omicron challenge. Nat. Commun. *13*, 3589.

Zost, S.J., Gilchuk, P., Case, J.B., Binshtein, E., Chen, R.E., Nkolola, J.P., Schäfer, A., Reidy, J.X., Trivette, A., Nargi, R.S., et al. (2020). Potently neutralizing and protective human antibodies against SARS-CoV-2. Nature *584*, 443–449.

Please cite this article in press as: Wang et al., Antigenic characterization of the SARS-CoV-2 Omicron subvariant BA.2.75, Cell Host & Microbe (2022), https://doi.org/10.1016/j.chom.2022.09.002

STAR★METHODS

KEY RESOURCES TABLE

REAGENT or RESOURCE	SOURCE	IDENTIFIER
Antibodies		
C1717	Wang et al., 2022d	N/A
S3H3	Hong et al., 2022	N/A
CAB-A17	Sheward et al., 2022	N/A
CB6	Shi et al., 2020 Provided by P. Kwong (NIH)	N/A
Brii-196	Ju et al., 2020	N/A
Omi-3	Nutalai et al., 2022	N/A
Omi-18	Nutalai et al., 2022	N/A
XGv347	Wang et al., 2022a	N/A
ZCB11	Zhou et al., 2022 Provided by Z. Chen (HKU)	N/A
S2E12	Starr et al., 2021	N/A
A19-46.1	Wang et al., 2021	N/A
COV2-2196	Zost et al., 2020 Provided by Regeneron Pharmaceuticals	N/A
LY-CoV555	Jones et al., 2021	N/A
REGN10933	Hansen et al., 2020 Provided by Regeneron Pharmaceuticals	N/A
XGv282	Wang et al., 2022a	N/A
LY-CoV1404	Westendorf et al., 2022	N/A
S309	Pinto et al., 2020	N/A
35B5	Wang et al., 2022c	N/A
JMB2002	Yin et al., 2022	N/A
COV2-2130	Zost et al., 2020 Provided by Regeneron Pharmaceuticals	N/A
REGN10987	Hansen et al., 2020 Provided by Regeneron Pharmaceuticals	N/A
Brii-198	Ju et al., 2020	N/A
10-40	Liu et al., 2022a	N/A
Bacterial and virus strains		
VSV-G pseudotyped ΔG-luciferase	Kerafast	Cat#EH1020-PM
Biological samples		
Boosted sera	Wang et al., 2022b	N/A
BA.1 breakthrough sera	Wang et al., 2022b	N/A
BA.2 breakthrough sera	Wang et al., 2022b	N/A
Chemicals, peptides, and recombinant proteins		
Polyethylenimine (PEI)	Polysciences Inc.	Cat#23966-100
hACE2	This paper	N/A
SARS-CoV-2 D614G S2P	Wang et al., 2022b	N/A
SARS-CoV-2 BA.2 S2P	Wang et al., 2022b	N/A
SARS-CoV-2 BA.4/5 S2P	Wang et al., 2022b	N/A
SARS-CoV-2 BA.2.75 S2P	This paper	N/A

(*Continued on next page*)

Please cite this article in press as: Wang et al., Antigenic characterization of the SARS-CoV-2 Omicron subvariant BA.2.75, Cell Host & Microbe (2022), https://doi.org/10.1016/j.chom.2022.09.002

Continued

REAGENT or RESOURCE	SOURCE	IDENTIFIER
Critical commercial assays		
Luciferase Assay System	Promega	Cat#E4550
QuikChange Lightning Site-Directed Mutagenesis Kit	Agilent	Cat#210518
Series S sensor chip CM5	Cytiva	Cat#BR100530
His-capture kit	Cytiva	Cat#28995056
Experimental models: cell lines		
HEK293T	ATCC	Cat#CRL-3216; RRID: CVCL_0063
Vero-E6	ATCC	Cat#CRL-1586; RRID: CVCL_0574
Expi293 cells	Thermo Fisher Scientific	Cat#A14527; RRID: CVCL_D615
Recombinant DNA		
pCMV3-D614G	Wang et al., 2022b	N/A
pCMV3-BA.2	Wang et al., 2022b	N/A
pCMV3-BA.2.12.1	Wang et al., 2022b	N/A
pCMV3-BA.4/5	Wang et al., 2022b	N/A
pCMV3-BA.2.75	This paper	N/A
pCMV3-D614G-K147E	This paper	N/A
pCMV3-D614G-W152R	This paper	N/A
pCMV3-D614G-F157L	This paper	N/A
pCMV3-D614G-I210V	This paper	N/A
pCMV3-D614G-G257S	This paper	N/A
pCMV3-D614G-G339H	This paper	N/A
pCMV3-D614G-G446S	This paper	N/A
pCMV3-D614G-N460K	This paper	N/A
pCMV3-BA.2-K147E	This paper	N/A
pCMV3-BA.2-W152R	This paper	N/A
pCMV3-BA.2-F157L	This paper	N/A
pCMV3-BA.2-I210V	This paper	N/A
pCMV3-BA.2-G257S	This paper	N/A
pCMV3-BA.2-D339H	This paper	N/A
pCMV3-BA.2-G446S	This paper	N/A
pCMV3-BA.2-N460K	This paper	N/A
pCMV3-BA.2-R493Q	This paper	N/A
paH-D614G S2P	Wang et al., 2022b	N/A
paH-BA.2 S2P	Wang et al., 2022b	N/A
paH-BA.4/5 S2P	Wang et al., 2022b	N/A
paH-BA.2.75 S2P	This paper	N/A
pcDNA3-sACE2-WT(732)-IgG1	Chan et al., 2020	RRID: Addgene_154104
Software and algorithms		
GraphPad Prism 9	GraphPad Software Inc	https://www.graphpad.com/scientific-software/prism/
PyMOL v.2.3.2	Schrödinger, LLC	https://pymol.org/2/#page-top
Biacore T200 Evaluation Software (Version 1.0)	Cytiva	NA

Please cite this article in press as: Wang et al., Antigenic characterization of the SARS-CoV-2 Omicron subvariant BA.2.75, Cell Host & Microbe (2022), https://doi.org/10.1016/j.chom.2022.09.002

RESOURCE AVAILABILITY

Lead contact

Further information and requests for resources and reagents should be directed to and will be fulfilled by the Lead Contact Author David D. Ho (dh2994@cumc.columbia.edu).

Materials availability

All reagents generated in this study are available from the Lead Contact with a completed Materials Transfer Agreement.

Data and code availability

- Data reported in this paper will be shared by the lead contact upon request.
- This paper does not report original code.
- Any additional information required to reanalyze the data reported in this paper is available from the lead contact upon request.

EXPERIMENTAL MODEL AND SUBJECT DETAILS

Patients and vaccinees

Sera from individuals who received three doses of the mRNA-1273 or BNT162b2 vaccines were collected at Columbia University Irving Medical Center (referred to as "boosted" in the text). Sera from individuals who were infected by an Omicron subvariant (BA.1 or BA.2) following vaccinations were collected from December 2021 to May 2022 at Columbia University Irving Medical Center (referred to as "BA.1 or BA.2 breakthrough" in the text). All samples were confirmed for prior SARS-CoV-2 infection status by anti-nucleoprotein (NP) enzyme-linked immunosorbent assay (ELISA), and the variant involved in breakthrough cases was determined by sequencing. All collections were conducted under protocols reviewed and approved by the Institutional Review Board of Columbia University. All participants provided written informed consent. Clinical information on the different cohorts of study subjects is provided in Table S1.

Cell lines

Expi293 cells were obtained from Thermo Fisher Scientific (A14527); Vero-E6 cells were obtained from the ATCC (CRL-1586); HEK293T cells were obtained from the ATCC (CRL-3216). Expi293 cells were maintained in Expi293^{TM} Expression Medium, supplemented with 0.5% penicillin-streptomycin (Thermo Fisher Scientific, Cambridge, MA), and were incubated at 37°C, 8% CO_2, 125 rpm. Vero-E6 and HEK293T cells were cultured in Dulbecco modified Eagle medium (DMEM) supplemented with 10% fetal bovine serum (FBS) and 1% penicillin-streptomycin at 37°C, 5% CO_2. HEK293T cells and Expi293 cells are of female origin. Vero-E6 cells are from African green monkey kidneys. Cells were purchased from authenticated vendors and morphology was confirmed visually before use. All cell lines tested mycoplasma negative.

METHOD DETAILS

Monoclonal antibodies

Antibodies were expressed in-house as previously described (Liu et al., 2020). For each of the antibodies in this study, heavy chain variable (VH) and light chain variable (VL) genes were synthesized (GenScript), cloned into an expression vector, transfected into Expi293 cells (Thermo Fisher Scientific), and purified from the cellular supernatant by affinity purification using rProtein A sepharose (GE). REGN10987, REGN10933, COV2-2196, and COV2-2130 were provided by Regeneron Pharmaceuticals; Brii-196 and Brii-198 were provided by Brii Biosciences; CB6 was provided by B. Zhang and P. Kwong (NIH); and ZCB11 was provided by Z. Chen (HKU).

Construction of SARS-CoV-2 spike plasmids

Spike expression constructs for D614G, BA.2, BA.2.12.1, and BA.4/5 were previously generated (Iketani et al., 2022; Liu et al., 2022b; Wang et al., 2022b). Expression constructs encoding the BA.2.75 spike, as well as the individual mutations found in BA.2.75, were generated using the QuikChange II XL site-directed mutagenesis kit according to the manufacturer's instructions (Agilent). For expression of stabilized soluble S2P spike trimer proteins, 2P substitutions (K986P and V987P in WA1) and a "GSAS" substitution of the furin cleavage site (682-685aa in WA1) were introduced into the spike-expressing plasmids for stabilization as previously described (Wrapp et al., 2020), and then the ectodomain (1-1208aa in WA1) of the spike was fused with a C-terminal 8x His-tag and cloned into the paH vector. All constructs were confirmed by Sanger sequencing prior to use.

Expression and purification of SARS-CoV-2 stabilized spike trimers and human ACE2

Stabilized SARS-CoV-2 spike trimer proteins of D614G and the Omicron subvariants were generated by transfecting Expi293 cells with each of the stabilized spike trimer expression constructs using 1 mg mL^{-1} polyethylenimine (PEI), and then purifying the spike trimer from the supernatants five days post-transfection using nickel-nitrilotriacetic acid (Ni-NTA) resin (Invitrogen) according to the manufacturer's instructions (Liu et al., 2020). Dimeric human ACE2-IgG1 (hACE2) was generated by transfecting Expi293 cells with

pcDNA3-sACE2-WT(732)-IgG1 (Chan et al., 2020) (Addgene plasmid #154104, gift from Erik Procko) using 1 mg mL^{-1} PEI and then purifying from the supernatant five days post-transfection using rProtein A sepharose (GE) according to the manufacturer's instructions. All proteins were confirmed for purity and size by sodium dodecyl-sulfate polyacrylamide gel electrophoresis (SDS-PAGE) prior to use.

Surface plasmon resonance (SPR)

Surface plasmon resonance binding assays for hACE2 binding to SARS-CoV-2 stabilized spike trimers were performed using a Biacore T200 biosensor equipped with a Series S CM5 chip (Cytiva), in a running buffer of 10 mM N-2-hydroxyethylpiperazine-N'-2-ethanesulfonic acid (HEPES) pH 7.4, 150 mM NaCl, 3 mM ethylenediaminetetraacetic acid (EDTA), 0.05% P-20 (Cytiva) at 25 °C. Spike proteins were captured through their C-terminal His-tag over an anti-His antibody surface. These surfaces were generated using the His-capture kit (Cytiva) according to the manufacturer's instructions, resulting in approximately 10,000 resonance units (RU) of anti-His antibody over each surface. An anti-His antibody surface without antigen was used as a reference flow cell to remove bulk shift changes from the binding signal. For each spike, binding to hACE2 was tested using a three-fold dilution series with concentrations ranging from 2.46 nM to 200 nM. The association and dissociation rates were each monitored for 60 s and 600 s respectively, at 30 μL/min. The bound spike/hACE2 complex was regenerated from the anti-His antibody surface using 10 mM glycine pH 1.5. Blank buffer cycles were performed by injecting running buffer instead of hACE2 remove systematic noise from the binding signal. The resulting data was processed and fit to a 1:1 binding model using Biacore Evaluation Software.

Pseudovirus production

Pseudotyped SARS-CoV-2 (pseudoviruses) were produced in the vesicular stomatitis virus (VSV) background, in which the native VSV glycoprotein was replaced by that of SARS-CoV-2 and its variants, as previously described (Liu et al., 2020). HEK293T cells were transfected with the appropriate spike expression construct using 1 mg mL^{-1} PEI and cultured overnight at 37 °C under 5% CO_2, and then infected with VSV-G pseudotyped ΔG-luciferase (G*ΔG-luciferase, Kerafast) 24 h post-transfection. After 2 h of infection, cells were washed three times, changed to fresh medium, and then cultured for approximately another 24 h before the supernatants were collected, clarified by centrifugation, and aliquoted and stored at -80 °C until further use.

Pseudovirus neutralization assay

Prior to use in the neutralization assay, all pseudoviruses were first titrated to equilibrate the viral input between assays. Five-fold serial dilutions of heat-inactivated sera, antibodies, or hACE2 were prepared in media in 96-well plates in triplicate, starting at 1:100 dilution for sera and 10 μg mL^{-1} for antibodies and hACE2. Pseudoviruses were then added to wells and the virus–sample mixture was incubated at 37 °C for 1 h, except for hACE2, where no incubation was conducted. Control wells with the virus only were included on all plates. Vero-E6 cells were then added at a density of 3×10^4 cells per well and the plates were incubated at 37 °C for approximately 10 h. Cells were then lysed and luciferase activity was quantified using the Luciferase Assay System (Promega) according to the manufacturer's instructions with SoftMax Pro v.7.0.2 (Molecular Devices). Neutralization curves and IC_{50} values were derived by fitting a nonlinear five-parameter dose-response curve to the data in GraphPad Prism v.9.2.

Structural modeling of RBD mutations

The structures of antibody-spike complexes for modeling were obtained from PDB (PDB: 7WLC (XGv282), PDB: 7XOD (JMB2002), PDB: 7C01 (CB6), PDB: 7ZF3 (Omi-3), and PDB: 7ZFB (Omi-18)). PyMOL v.2.3.2 was used to perform mutagenesis, to identify steric clashes and hydrogen bonds between RBD and antibodies, and to generate structural plots (Schrödinger, LLC).

QUANTIFICATION AND STATISTICAL ANAYLYSIS

Serum neutralization ID_{50} values and antibody and hACE2 neutralization IC_{50} values were calculated using a five-parameter dose-response curve in GraphPad Prism v.9.2. Evaluations of statistical significance were performed employing two-tailed Wilcoxon matched-pairs signed-rank tests using GraphPad Prism v.9.2 software. Levels of significance are indicated as follows: ns, not significant; *, $P < 0.05$; **, $P < 0.01$; ***, $P < 0.001$; and ****, $P < 0.0001$. The SPR data was processed and fit to a 1:1 binding model using Biacore Evaluation Software.